Materials Today Physics 18 (2021) 100378

Contents lists available at ScienceDirect

Materials Today Physics

journal homepage: https://www.journals.elsevier.com/materials-today-physics

Recent progress on two-dimensional layered materials for surface enhanced Raman spectroscopy and their applications

Zhen Yin [a, b], Kaichen Xu [c, **], Shouzhen Jiang [d], Dan Luo [a], Rui Chen [a], Chunxiang Xu [b], Ping Shum [a], Yan Jun Liu [a, e, *]

[a] Department of Electrical and Electronic Engineering, Southern University of Science and Technology, Shenzhen, 518055, China
[b] State Key Laboratory of Bioelectronics, Southeast University, Nanjing, 210096, China
[c] State Key Laboratory of Fluid Power and Mechatronic Systems, School of Mechanical Engineering, Zhejiang University, Hangzhou, 310027, China
[d] Shandong Provincial Key Laboratory of Optics and Photonic Device, School of Physics and Electronics, Shandong Normal University, Jinan, 250014, China
[e] Key Laboratory of Energy Conversion and Storage Technologies (Southern University of Science and Technology), Ministry of Education, Shenzhen, 518055, China

ARTICLE INFO

Article history:
Received 27 December 2020
Received in revised form
25 February 2021
Accepted 1 March 2021
Available online 2 March 2021

Keywords:
SERS
2D materials
Plasmonics
Heterostructures
Hot spot

ABSTRACT

Surface-enhanced Raman spectroscopy (SERS) has become an ultrasensitive technique in trace molecule detection through its unique vibrational fingerprint. However, development of a SERS platform with large enhancement factor, superior stability, and excellent reproducibility is still a grand challenge for practical applications. Recently, two-dimensional (2D) materials play an intriguing role for SERS through the use of their unique structures and properties. This review summarizes the recent progress of 2D materials-based SERS that could be complements to plasmonic SERS substrates. Based on the symmetry of the lattice structure, isotropic and anisotropic 2D materials for SERS are introduced. Particularly, various methods to improve the SERS performance are described. The sensitivity, limit of detection, and stability are discussed for 2D materials-based heterostructures as SERS platforms, including van der Waals and hybrid heterostructures. Furthermore, the applications of 2D materials-based SERS substrates in niche areas, including local strain probing, remote/in-situ chemical analysis, and fine structure characterization are summarized.

1. Introduction

In the past two decades, the rapid development of nanotechnology has ceaselessly pushed forward the dramatic advances in diverse functional physical and chemical sensors for a wide variety of applications, such as healthcare diagnostics, environment monitoring, national security, and food quality analyses [1–4]. Among many sensing techniques, surface-enhanced Raman spectroscopy (SERS) has presented its significant role as an ultrasensitive route in trace molecule detection through its unique vibrational fingerprint [5]. The enhancement effect of SERS is primarily attributed to the interplay between the electromagnetic mechanism (EM) and the chemical mechanism (CM) [6]. The EM originates from the enhanced localized electromagnetic field near plasmonic nanoparticles or roughened surface (tens to hundreds nanometers in surface roughness) [7] owing to surface plasmon resonances (SPRs) [8–13]. While the CM is highly dependent on the coupling between the substrate and absorbed molecules through charge transfer and the mixing of molecular orbitals with electronic states [14]. Generally, EM plays the dominant role for metallic SERS substrates with an enhancement factor of 10^6–10^{10} [15–20], however, the issues including stability, biological compatibility, and strong spectral background of metallic SERS substrates have greatly limited their applications [21–25]. Instead, non-metallic materials could enable not only more efficient EM enhancement with low damping rates and reduced Ohmic loss [26,27], but also high CM enhancement due to the enhanced charge transfer [28]. Consequently, non-metallic materials are considered as an excellent complement for SERS.

Since the discovery of graphene in 2004 [29], the booming development of two-dimensional (2D) layered nanomaterials, such as transition-metal dichalcogenides (TMDCs), hexagonal boron

* Corresponding author. Department of Electrical and Electronic Engineering, Southern University of Science and Technology, Shenzhen, 518055, China.
** Corresponding author.
E-mail addresses: xukc@zju.edu.cn (K. Xu), yjliu@sustech.edu.cn (Y.J. Liu).

https://doi.org/10.1016/j.mtphys.2021.100378
2542-5293/

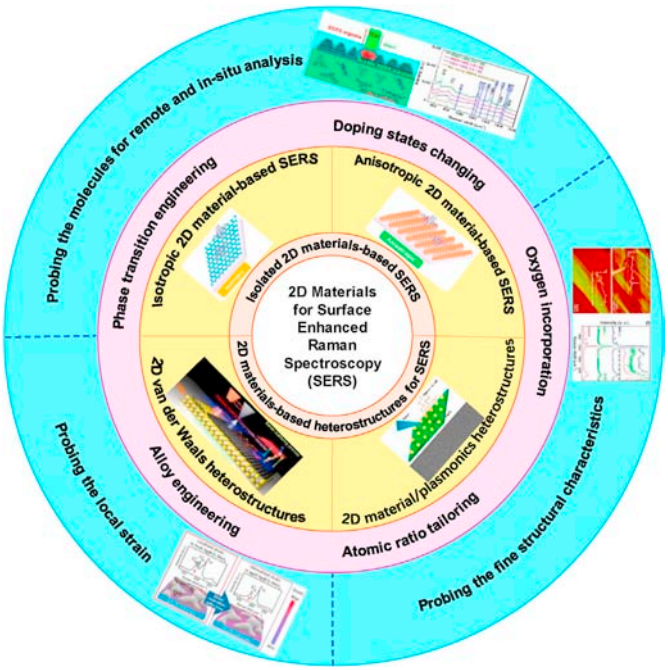

Fig. 1. Overview of 2D materials-based surface enhanced Raman scattering. Adapted from Ref. [35], with permission from © 2015 American Chemical Society. Adapted from Ref. [36], with permission from © 2017 American Chemical Society. Adapted from Ref. [37], with permission from © 2017 American Chemical Society. Adapted from Ref. [38], with permission from © 2018 American Chemical Society. Adapted from Ref. [39], with permission from © 2009 American Chemical Society. Adapted from Ref. [40], with permission from © 2018 Elsevier Ltd.

nitride (h-BN), and black phosphorus, has provided versatile resources for the CM-based SERS research. Compared with noble metals, 2D materials have significant merits of high uniformity, better chemical stability and biocompatibility, rendering them promising for SERS [30,31]. Generally, 2D materials can be served as complements to metallic SERS, holding a crucial role for extending the capabilities of SERS and harnessing their huge potentials in many fields.

So far, significant progress has been made regarding 2D materials-based SERS, graphene or other 2D materials have been mentioned tin previous reviews [32–34]. To further give a better bird view of this field, it becomes crucial to highlight recent progress in 2D materials-based SERS that renders a deeper understanding of the CM process and resulted new possibilities for SERS applications.

In this review, we summarize the 2D materials-based SERS into four main sections, as presented in Fig. 1. In the first section, the fundamentals of 2D materials-based SERS, including charge-transfer and exciton resonances, are introduced. The second section divides the 2D materials-based SERS substrates into isotropic and anisotropic based on the structural symmetry. Particularly, various methods to enhance the SERS performance of 2D materials are discussed. In the third section, 2D materials-based heterostructures as SERS platforms are discussed in detail. Finally, 2D materials-based SERS applications in niche fields, particularly including local strain probing, remote/in-situ chemical analysis, and fine structure characterization are summarized.

2. Enhancement mechanisms of 2D materials-based SERS substrates

Unlike EM enhancement of most plasmonic SERS substrates, the 2D materials-based ones are generally attributed to CM enhancement, which is a short-range effect, primarily depending on the amplification of the Raman polarizability tensor of molecules upon its chemisorption on the 2D material surface. For the molecule-2D material system, the CM enhancement arises mainly from the charge-transfer (CT) and exciton resonances.

2.1. Charge-transfer resonance

In a molecule-metal system, the CT process occurs between the metal and molecules, which is determined by the relative energies of the metal Fermi level, the highest occupied molecular orbital (HOMO) and the lowest unoccupied molecular orbital (LUMO) levels [41]. While in most molecule-2D material systems, there is an energy gap between a full valence band (VB) and an empty conduction band (CB), then the efficient CT process depends on good match of the orbital wave-functions and energies between the HOMO/LUMO frontier orbitals of the molecule and the VB/CB orbitals [42].

Fig. 2 shows the five paths of CT resonances in a 2D material-molecule system. In the first path (Fig. 2a), the molecular ground state electron transits from the HOMO level to an energy level of the CB in the 2D material under the influence of light radiation, and transfers back to a molecular ground vibrational energy level with a Raman scattered photon emission. In the second path (Fig. 2b), reduction of the CT complex formation occurs with the chemical bonding between the molecule and 2D material, leading to the amplification of the Raman polarizability tensor and the consequent Raman signals. In the third path (Fig. 2c), the valance electron of the 2D material is transited to the high energy LUMO level, then quickly travels back to the VB with a Raman scattered photon emission. For example, CT transitions from VB to LUMO for pristine MoS_2 occur at 1.80 eV, while for the oxygen-incorporated MoS_2, the corresponding CT transitions take place at 2.26 eV. The VB position are remarkably downshifted compared with that of pristine MoS_2, which makes its CT transition energy much closer to the excitation laser energy. The detection limit of Rhodamine 6G (R6G) is 10^{-7} M [22]. In the fourth path (Fig. 2d), a surface state is formed as the electron is excited from the VB of the 2D material to the surface defect, which is further transited from the surface state to the LUMO and emitting a Raman scattered photon by traveling back to the surface state. Furthermore, in the fifth path (Fig. 2e), the electron in some dye molecules can transit to a higher energy LUMO level upon light excitation, and can inject into the CB of 2D materials via resonant tunneling, which finally travels back to a ground vibrational energy level of the molecule with a Raman scattered emission. For instance, the chemical potential difference between ReS_2 and R6G allows the electrons of R6G pumped from the HOMO to LUMO level to efficiently transfer to the CB of ReS_2. The degree of CT transitions from R6G to ReS_2 is heavily influenced by the band structure of ReS_2. For monolayer ReS_2 SERS substrate, the detection limit of R6G is as low as 10^{-9} M [44].

2.2. Exciton resonance

Exciton resonance is a unique electronic feature for most 2D materials, which is of little concern in metallic SERS substrates. Excitons are the creation of electron–hole pairs in the 2D material bound by the Coulomb interaction when the electrons transmit from the VB into various exciton levels due to photon excitation. The excitonic features are usually distinct in 2D materials due to a higher exciton binding energy than bulk materials.

Energy levels and wave functions of excitons occur by the Coulomb attractive force between the electron and the hole. As the dimension of 2D material is comparable to the exciton Bohr radius

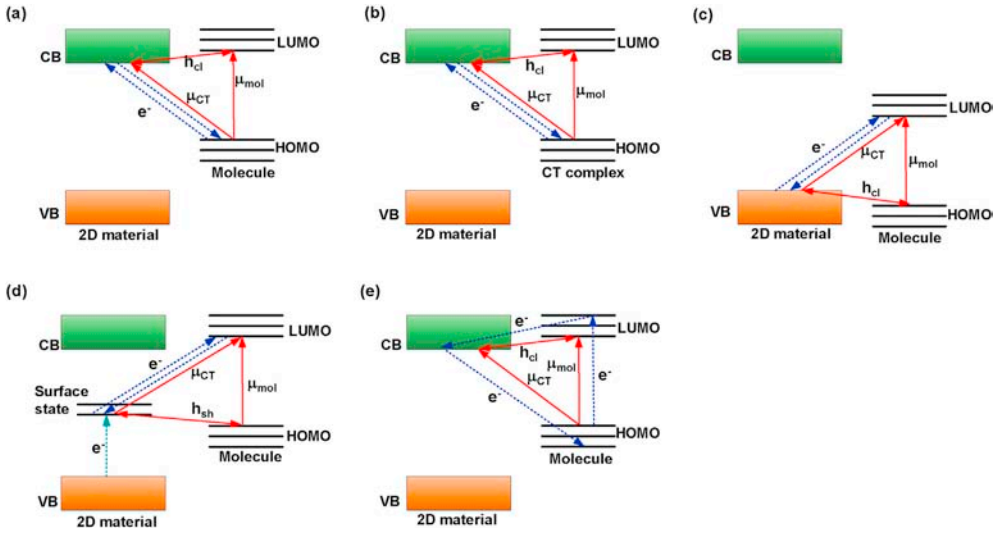

Fig. 2. The CT pathways in 2D material-molecule systems: (a) molecule HOMO-to-CB, (b) CT complex-to-CB, (c) VB-to-molecule LUMO, (d) surface state-to-molecule LUMO and (e) CB-to-molecule HOMO. Adapted from Ref. [43], with permission from © 2017 The Royal Society of Chemistry.

that is determined by the distance between an electron-hole pair, the exciton levels come to diverge by the quantum confinement effects [43]. For the exciton resonance excitation, it can give rise to sharply peak absorption features, and the Raman photon would irradiate when a vibrational quantum of energy transfers to the vibrational level of the molecule. Moreover, the exciton resonance as a source of intensity borrowing, can contribute to the SERS enhancement factor, and also affect the selection rules and the appearance of SERS spectrum [45], which can be effectively adjusted by the composition, environmental index, and electric/magnetic fields.

3. Isolated 2D materials-based SERS substrates

2D materials usually form strong chemical bonds in-plane but weak van der Waals bonding out-of-plane [46], and exhibit different symmetries including D_{6h} (graphene, $MoS(Se)_2$, $WS(Se)_2$, GaSe(S), and h-BN, etc.), D_{3d} ($SnSe_2$ and $Bi_2Te(Se)_3$), D_{2h} (black phosphorus (BP), GeS(Se), and SnS(Se)), C_{2h} (GaTe), and C_i ($ReS(Se)_2$) [47]. Among various symmetries of 2D materials, the lower symmetry (D_{2h}, C_{2h}, and C_i) induces the in-plane anisotropy, resulting in one more degree of freedom than isotropic materials and various physical properties [47]. According to the symmetries of crystal structures, the 2D material-based SERS substrates can be primarily divided into two types: isotropic and anisotropic ones.

3.1. Isotropic 2D materials-based SERS substrates

Until now, some important factors have been reported to be accountable for graphene-related SERS, including the first-layer effect [49] and doping states.[50–] [52] For instance, Ling et al. demonstrated the influence on the Raman signal by controlling of layer numbers and molecular configurations of the Langmuir–Blodgett (LB) film of protoporphyrin IX (PPP) (Fig. 3b_1 and 3b_2) [49], and the corresponding Raman spectra of PPP are shown in Fig. 3b_3–3b_5. Fig. 3b_6 shows the Raman intensity as a function of the layer number of PPP, where the first PPP monolayer had a dominant contribution to the Raman intensity. It is consistent with the "first-layer effect" [53], indicating the distance dependence of CT in the CM of SERS. Moreover, the Raman enhancement of molecules on graphene can be tuned by tailoring the graphene Fermi level under electrical field modulation (Fig. 3c_1). The Fermi level is equal to Dirac point for intrinsic single-layer graphene [54], which can be shifted below (above) the Dirac point due to the electrical field induced hole (electron) doping under a negative (positive) gate voltage (Fig. 3c_2). The Raman intensities of Copper phthalocyanine (CuPc) molecules can be reversibly modulated with an increasing percentage up to 29.7% (Fig. 3c_3), resulting from an enhanced CT resonance when the graphene Fermi level was down-shifted with a negative gate voltage, whereas they would get weaker due to the hindered CT resonance with a positive gate voltage. Moreover, the electric field induced modulation of CT enhancement in graphene-based SERS substrates is significantly influenced by the hysteresis effect, which can be suppressed under an n-doping atmosphere due to the different Fermi level modulation regions [51].

Beyond graphene, the Raman enhanced ability of other 2D materials, such as h-BN and TMDs, has been also explored, which have somewhat similar structures to graphene but different electronic and surface chemical properties. For h-BN, it is an insulator and has a strong B–N bond. The enhanced Raman signals of CuPc molecules are mainly attributed to the interface dipole interaction between h-BN and CuPc, which further induces an increased electron transition probability [55]. In addition, the enhanced Raman performance is independent of the thicknesses of h-BN due to its high transparency in the visible range. Moreover, MoS_2 is a semiconductor with the sulfur atoms on the surface and has a polar covalent bond (Mo–S) [56–58]. Compared with graphene and h-BN, both CT and interface dipole interaction contributions are much weaker. Consequently, it exhibits the weakest enhancement as a SERS substrate among these three 2D materials, which confirms the important role of CT in a conducting substrate.

The stability of 2D materials has a significant impact on the performance of the SERS substrates. On the one hand, 2D materials can protect analyte molecules, especially for dye molecules, from photoinduced damages, including photoinduced carbonization and photodegradation. For example, the R6G SERS signals from 1T/2H–MoS_2 and 1T/2H-WS_2 substrates were nearly unchanged up to 30 days, showing extraordinary stability against photothermal damages during laser excitation [59]. On the other hand, 2D materials can be also used as a shielding layer to protect metal substrates from oxidation. For instance, compared with bare Ag

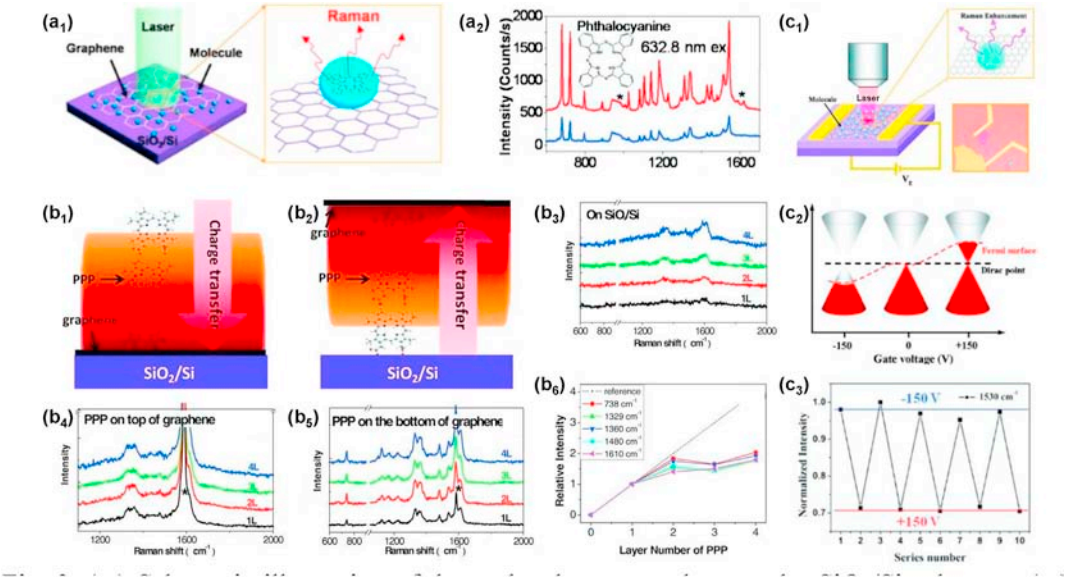

Fig. 3. (a_1) Schematic illustration of the molecules on graphene and a SiO_2/Si substrate. (a_2) Raman spectra of Pc molecules on graphene (red line) and on the SiO_2/Si substrate (blue line) under 632.8 nm laser excitation. Adapted from Ref. [48], with permission from © 2010 American Chemical Society. (b_1&b_2) Schematic diagrams of the contribution of the different numbers of PPP layers to the charge transfer between graphene and PPP. Raman spectra of PPP layers with different layer numbers on a blank SiO_2/Si substrate (b_3), and on the top (b_4) and the bottom (b_5) of graphene. (b_6) Raman intensities as a function of the layer number of the PPP film. Adapted from Ref. [49], with permission from © 2010 Wiley-VCH Verlag GmbH & Co. KGaA, Weinheim. (c_1) Schematic illustration of the experiment setup and an optical image of the graphene device. (c_2) Fermi level variation of single-layer graphene induced by electrical field. (c_3) Normalized Raman intensity variations of the C–N–C bridge vibration mode for the CuPc molecules. Adapted from Ref. [50], with permission from © 2011 American Chemical Society.

nanoparticles, the SERS signals from CVD-grown, graphene-coated Ag SERS substrate are stable up to 28 days with ambient aerobic exposure [60]. Moreover, the high-quality, large-scale 2D materials are also essential for practical applications with enhanced reproducibility and uniformity, which serve as ideal candidates for reliable monitoring [59,61]. For instance, the 1T/2H–MoS_2 nanosheet substrates with a working area of 3×4 cm^2 provide excellent uniformity and reproducibility for R6G detection [59].

3.2. Anisotropic 2D materials-based SERS substrates

Compared with the aforementioned isotropic 2D materials, the lately emerged anisotropic ones with lower symmetries not only exhibit unprecedented electrical and optical properties [62,63], but also possess unique in-plane anisotropy [64–66]. For example, compared to the isotropic ones, BP demonstrates distinct anisotropy of the polarization-dependent Raman enhancement (Fig. 4a) [35]. CuPc molecules are sandwiched between anisotropic BP and a blank SiO_2/Si substrate (Fig. 4b). Fig. 4c shows atomic structure of a single BP layer, which possesses anisotropic conductivity, photoelectric response and Raman scattering. As a result, there is 3–6 times Raman enhancement induced by the BP anisotropy compared to the blank SiO_2/Si substrate (Fig. 4d).

Typically, the Raman enhancement effect of 2D materials originates mainly from interfacial CT, the strength of which relies on the charge distribution on the substrate. For an anisotropic BP surface, the charges distribution is uniform, while with the contact of the CuPc molecules, the charges are redistributed into one-dimensional (1D) chains along armchair direction (Fig. 4e). The effective electron/hole mass along the AC direction is much smaller than that along zigzag (ZZ) direction, indicating that the charge carriers are mobile and diffuse much faster along the AC direction. Hence, the 2D materials display anisotropic carrier mobility. Under laser excitation, the most significant charge interaction across the interface occurs only for CuPc molecules with their primary axis along the armchair direction due to the anisotropic excitons for Raman enhancement (Fig. 4g). For an isotropic graphene surface, the charges are distributed isotropically both without and with CuPc molecules due to its high symmetry and isotropic electronic properties (Fig. 4f), and the charge interactions between graphene and CuPc molecules are also isotropic (Fig. 4h). Therefore, the Raman enhancement exhibits no angular dependence.

Similar results have been also observed on triclinic ReS_2, in which the charge distributions are primarily along the zigzag direction. Under laser irradiation, the charge carriers diffuse much faster along the zigzag direction due to the highest mobility, [67] and the strongest charge interaction also occurs across the interface when the primary axis of CuPc molecules is aligned in zigzag direction, leading to the strongest Raman enhancement. However, the anisotropic Raman enhancement is highly dependent on this small portion of specifically oriented molecules. As a result, the overall Raman enhancement factor of CuPc molecules on ReS_2 is only less than 10 due to the low proportion of the effective CuPc molecules. These results not only provide a new approach to understand the fundamental principles of CM process for SERS enhancement, but also add an additional dimension based on the symmetry of the SERS substrate.

3.3. SERS performance enhancement of 2D materials

To improve the SERS performance of 2D materials, several methods have been exploited currently including doping states modification, oxygen incorporation, phase transition engineering, alloy engineering and atomic ratio tailoring. For instance, Feng et al. demonstrated a better SERS effect based on the enhanced CT processes of graphene by controlling nitrogen doping. Since the Fermi level of graphene shift aligned with the LUMO of the detecting molecule, the molecule's vibrational Raman modes will be amplified significantly. The detection limit for Rhodamine B molecules can be down to 5×10^{-11} M [68]. Moreover, the CT of MoS_2 can be

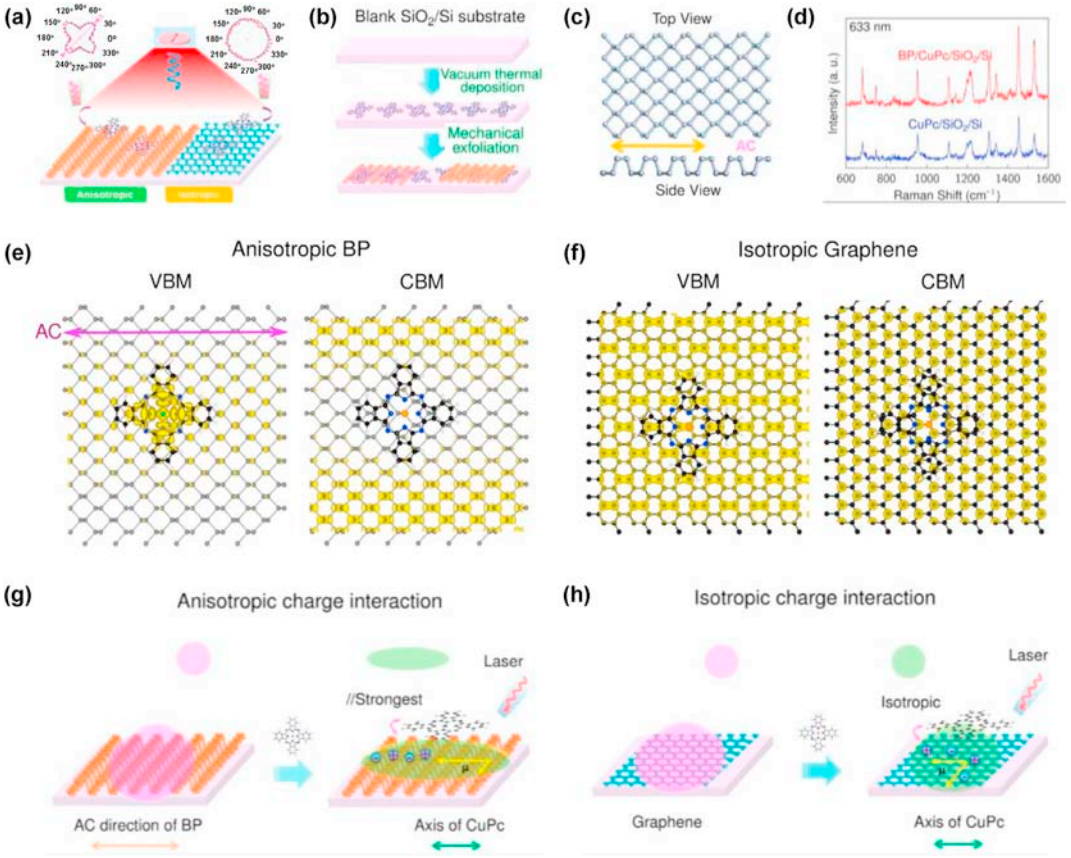

Fig. 4. (a) Anisotropy and isotropy of Raman enhancement corresponding to anisotropic and isotropic 2D materials, respectively. (b) Schematic illustration of the sample preparation procedure. (c) Top and side views of orthorhombic BP. The yellow double arrow represents the armchair direction of BP. (d) Raman spectra of CuPc molecules on SiO_2/Si substrate (red) and with BP covered on top (blue). (e, f) Charge distributions of electronic bands near the Fermi level for (e) CuPc/BP, (f) CuPc/graphene systems. (g, h) Schematic illustration of anisotropic and isotropic charge interaction processes in (g) CuPc/BP and (h) CuPc/graphene systems, respectively. Adapted from Ref. [35], with permission from © 2015 American Chemical Society.

enhanced through synergistic structural and electronic modulations by oxygen incorporation, making its CT transition energy much closer to the excitation laser energy, which is an efficient pathway for improving the enhanced Raman performance of some 2D materials. As long as the phase structure of oxygen-incorporated MoS_2 remains undisrupted with rising oxygen-incorporated concentrations, the Raman enhancement factors can be up to 10^5 with the detection limit of R6G down to 10^{-7} M [22], due to the enhanced CT and exciton resonances by controlling oxygen-incorporated concentration in 2D materials.

Additionally, the CT process for SERS can be greatly enhanced via the phase transition of TMDCs from semiconducting 2H- to metallic 1 T-phase, due to the more efficient electron transfer from the Fermi level of metallic 1 T-MoX_2 to the HOMO level than semiconducting 2H-MoX_2. The enhancement factor of metallic 1 T-phase samples is at least one order of magnitude higher than the 2H-counterparts [69]. Moreover, the proportion of metallic phase of 2D materials plays an important role on the SERS performances. The CT process of metallic 2D SERS substrate can be enhanced by abundant density of states near the Fermi level, which can increase the intermolecular CT probability. For example, Song et al. demonstrated that metallic 2D NbS_2 with large abundant density of states could be used as an excellent plasmon-free SERS substrates with a detection limit of methylene blue down to 10^{-14} M [70]. Furthermore, the SERS activity of 2D materials can be tuned by tailoring the atomic ratio. In 2018, Liu et al. demonstrated that the SERS performance for the CuPc molecules on the WSe_2 monolayers with a reduced atomic ratio (Se:W) of 1.96 was 40 times higher than that of pristine WSe_2, due to the enhanced exciton and CT resonances [71]. More recently, Hou et al. reported the manganese phosphorus trichalcogenides ($MnPS_{3-x}Se_x$, $0 \leq x \leq 3$) as a SERS-active substrate by alloy engineering, which showed a detection limit for R6G down to 10^{-9} M, due to the coupling between CT and exciton resonance [72].

Furthermore, defect is crucial for tuning the chemical, optical, and electronic properties of 2D materials, which can adjust the performance of 2D materials in SERS sensing. For example, femtosecond laser irradiation induced micro/nanodefects sites can facilitate the adsorption of molecules and even create local dipoles, resulting in enhanced charge transfer and the interface dipole−dipole coupling between R6G molecules on MoS_2 [57]. This would enhance the CM effect of 2D materials for SERS detection. Besides, as Se point defects were formed via Ga ion irradiation in a vertical WSe_2/Graphene heterostructure, it would provide higher transfer rate for out-of-plane charge transport and more electronic states for photoexcitation, leading to enhanced photoinduced interlayer charge transfer [73]. Moreover, for vertical few-layer MoS_2 nanosheet substrates, the abundant aligned edges act as active sites for MoS_2-molecule interaction, which not only contribute to sufficient contact and adsorbance of analytes for the excellent Raman enhancement, but also suppress the fluorescent background, synergistically facilitating the outstanding Raman readout [59].

4. 2D materials-based heterostructures for SERS

Compared with isolated 2D materials, heterostructured SERS platforms provide superior performance in terms of sensitivity, detection limit and stability. When different 2D materials are reassembled by stacking layer by layer vertically without strong interactions among them, forming van der Waals heterostructures, they can provide new functionalities due to the mutual complementarity of different 2D materials. Moreover, combining 2D materials with metallic nanostructures, 2D material/metal heterostructures are formed that can induce a much higher enhancement effect than sole metallic SERS substrates due to the synergistic EM and CM effects. Furthermore, 2D materials can also serve as protective layers to improve the stability and repeatability of SERS substrates. The following discussion focuses on 2D material van der Waals heterostructures and 2D material/metal heterostructures for SERS.

4.1. 2D material van der Waals heterostructures

For van der Waals layer-stacked heterostructures, the interlayer interaction is predominated by van der Waals force [74], permitting electron tunneling with no or little required lattice matching between neighboring layers [75]. The heterostructure allows the interlayer charge carriers flow with unique features. In addition, the heterostructure serves as a novel SERS platform for functional complementarity between different 2D materials. For example, Tan et al. reported the SERS performance of different heterostructures stacked by WSe_2 (W) and graphene (G) [36]. Fig. 5a shows the heterostructure with the graphene assembled on WSe_2 (G/W), and the enhanced Raman scattering can be attributed to the interlayer coupling via increased CT process, leading to an enriched electronic state density. Then, CuPc molecules were selected as the probing analyte by the LB technique. From Fig. 5b, it is obvious that the G/W heterostructure has the strongest Raman signal than their respective isolated counterpart, which can be also revealed obviously from the Raman mapping difference (Fig. 5c).

Additionally, the Raman enhancement effect of the van der Waals heterostructures depends largely on artificially stacked sequence of different 2D materials, such as the WSe_2 monolayer placed on top of graphene (W/G) (Fig. 5d), the interval stacked heterostructure (G/W/G/W) (Fig. 5e), the heterostructure with two graphene layers sandwiched between two WSe_2 layers (W/G/G/W) (Fig. 5f), resulting in different electronic structures. Fig. 5g–5i shows that the G/W heterostructure has the strongest Raman intensity, while the G/W/G/W heterostructure has a comparable enhancement effect compared to the G/W one (Fig. 5e). Moreover, both W/G and W/G/G/W heterostructures demonstrate stronger enhancement than the isolated one (Fig. 5g and i) due to its lower interlayer coupling efficiency related to different electron transition probability rates.

In addition, Seo et al. reported graphene/ReO_xS_y heterostructure as an ultrasensitive SERS substrate due to the synergistic effects of CT and exciton resonances [76]. Fig. 6a shows the van der Waals heterostructure consisting of graphene and ReO_xS_y film and its SERS effect. The measured SESR spectra of R6G with concentrations changing from 10^{-4} to 10^{-15} M are shown in Fig. 6b. Moreover, the SERS intensities are gradually reduced with decreased concentrations, and the detection limit of the substrate is down to 10^{-15} M (Fig. 6c). More recently, Dandu and co-workers reported that MoS_2/$SnSe_2$ and MoS_2/h-BN/$SnSe_2$ van der Waals heterostructures demonstrated 10-fold enhanced SERS activity due to nonradiative energy transfer [77]. Therefore, the van der Waals heterostructures provide excellent platforms for molecular Raman signal enhancement through the enhanced CM effect.

4.2. 2D material/metal heterostructures

As the EM enhancement factor is significantly higher than the CM one, metallic nanoparticles or nanostructures can be exploited

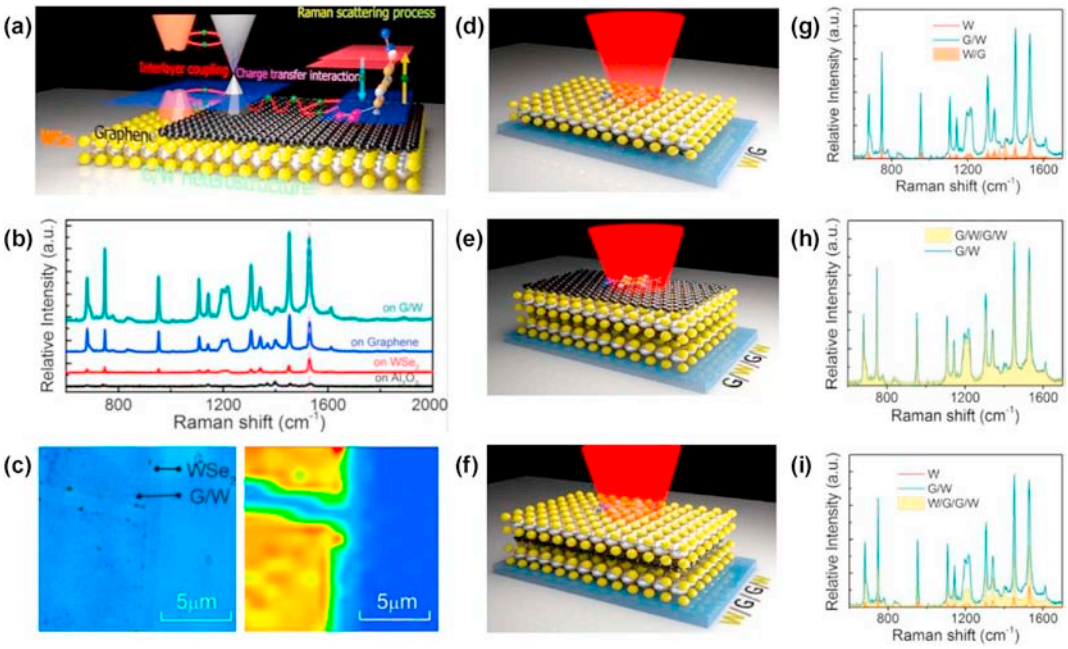

Fig. 5. (a) Schematic diagram of electronic transitions in the G/W heterostructure. (b) Raman spectra of the CuPc molecules on Al_2O_3 wafer, WSe_2, graphene, and G/W, respectively. (c) The optical image (left) and the corresponding Raman mapping image (right) for the CuPc molecules at 1528.3 cm-1 (d–f) Schematic illustration of different heterostructures of (d) W/G, (e) G/W/G/W, and (f) W/G/G/W, respectively. (g–i) Raman spectra of the CuPc molecules on (g) W/G, (h) G/W/G/W, and (i) W/G/G/W heterostructures. Adapted from Ref. [36], with permission from © 2017 American Chemical Society.

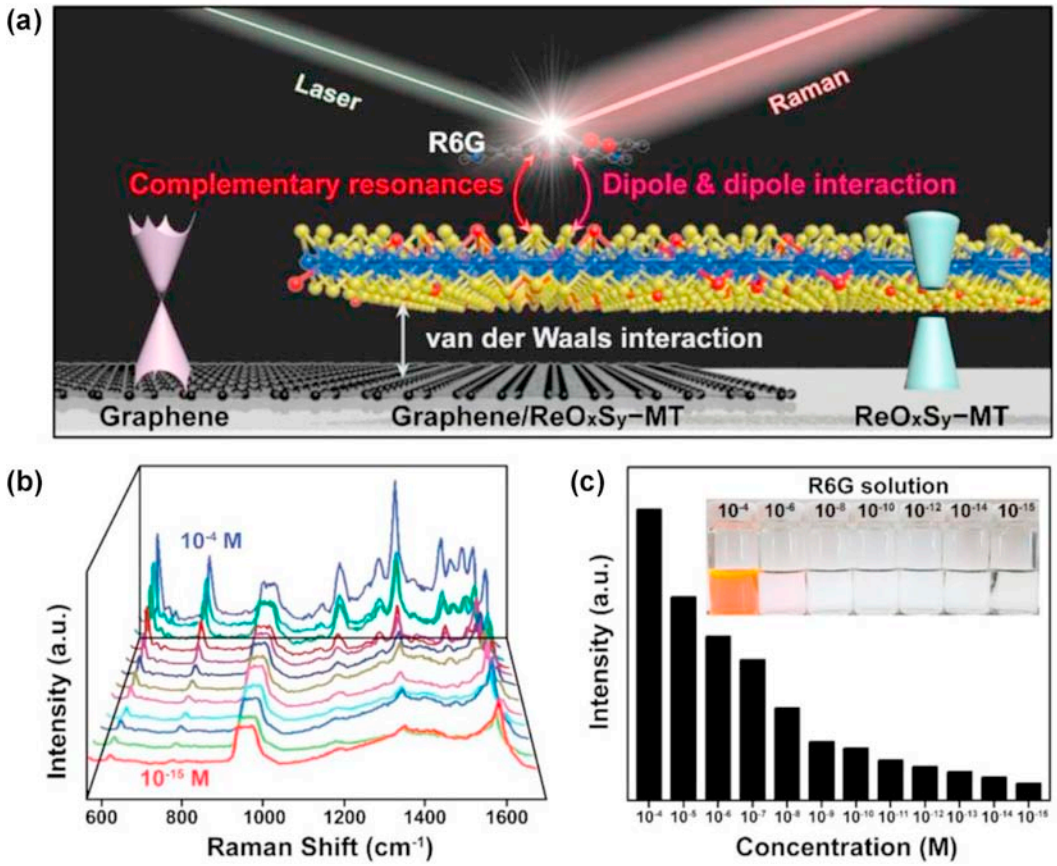

Fig. 6. (a) Schematic of the graphene/ReO_xS_y heterostructure. (b) SERS spectra of R6G with concentrations from 10^{-4} to 10^{-15} M. (c) The corresponding SERS signal intensity at 614 cm^{-1} as a function of decreased R6G concentrations. Adapted from Ref. [76] with permission from © 2017 American Chemical Society.

to increase the Raman enhancement effect of 2D materials. The heterostructures of 2D materials and metallic nanoparticles (nanostructures) as hybrid SERS substrates open up a new prospect to enhance the SERS performance. For instance, the enhancement factor for detection of R6G molecules from the AuNPs/graphene SERS substrate that fabricated by in situ self-assembly of Au nanoparticles (AuNPs) on isotropic graphene (Fig. 7a_1) is 4 times larger than the Au alone SERS substrate (Fig. 7a_2) [78]. As for quantitative study of such AuNPs/graphene SERS substrates, both the graphene and the AuNPs play a synergistic effect for the Raman enhancement, where the former exploits the strong CM enhancement from R6G molecule−graphene interactions, while the latter makes use of plasmonic EM enhancement due to the LSPR effect (Fig. 7b_1). The detection limit for R6G molecules is as low as 8×10^{-7} M (Fig. 7b_2) [79]. Furthermore, Chen et al. reported a stretchable hybrid SERS platform comprising of wrinkled graphene and Au NPs with the detection limit of R6G molecules down to 10^{-9} M [80], of which the wrinkled graphene acted as a thermal conductor and a protective layer of oxidation.

Since shell-isolated nanoparticle-enhanced Raman spectroscopy (SHINERS) was reported in 2010 [83], 2D materials with atomically thin and seamless nature have served as satisfying candidates compared to inert shell (*e.g.* SiO_2 or Al_2O_3) [84,85]. To avoid serious oxidative damage, Xu et al. reported monolayer graphene-wrapped Cu nanoparticles (Graphene/CuNPs) as a SERS substrate (Fig. 7c_1 and 7c_2) for the detection of adenosine with the ultralow concentration as low as 5 nM (Fig. 7c_3), which depended on the less loss of EM enhancement and molecules' adsorption of graphene [81]. In addition to graphene, graphene derivatives such as graphene oxide (GO), have superior biocompatibility, selective adsorption of molecules and chemical stability due to its rich hydrophilic oxygenated functional groups. For example, Liu's group used graphene oxide (GO)-decorated Ag dendritic (AgD) nanostructures on a copper substrate (GO/AgD/Cu) as a SERS platform (Fig. 7d_1), which exhibited superior SERS performance of sensitivity, signal-to-noise ratio and stability than non-decorated AgD [82]. The detection limit of R6G on GO/AgD/Cu substate can be down to 10^{-11} M, which is one order of magnitude lower than the non-decorated one (Fig. 7d_2 and 7d_3). Similar to the surface decoration of graphene, selectively assembled Au nanoparticles (NPs) on few-layer 2D MoS_2 film provide an efficient SERS substrate for aromatic molecules sensing. The Au NPs/MoS_2 SERS substrate shows high Raman enhancement of R6G with the detection limit down to 10^{-9} M, owing to the synergistic effects between the efficient adsorption of molecules and the strong plasmon coupling of the Au NPs [86]. In addition, Li et al. demonstrated the MoS_2 shell coated AuNPs hybrids as effective SERS substrates with the detection limit of R6G down to 10^{-10} M [87]. Moreover, Lu et al. reported that anisotropic 2D layered GaTe with a monoclinic structure (Fig. 7e_2) acted as a superior SERS substrate (Fig. 7e_1), due to its high-density surface detects for Au NPs decoration. The Au NPs/GaTa hybrid shows much stronger and higher signal-to-noise ratio than the isolated GaTa counterpart with the detection limit of R6G molecules down to 10^{-11} M (Fig. 7e_3) [37]. More recently, Xie et al. reported gold nanorods decorated 2D MXene (Ti_3C_2Tx) as an efficient SERS substrate to analyze organic pollutants with the detection limit of thiram down to 10^{-10} M [88].

To achieve the SERS substrates with a higher enhancement

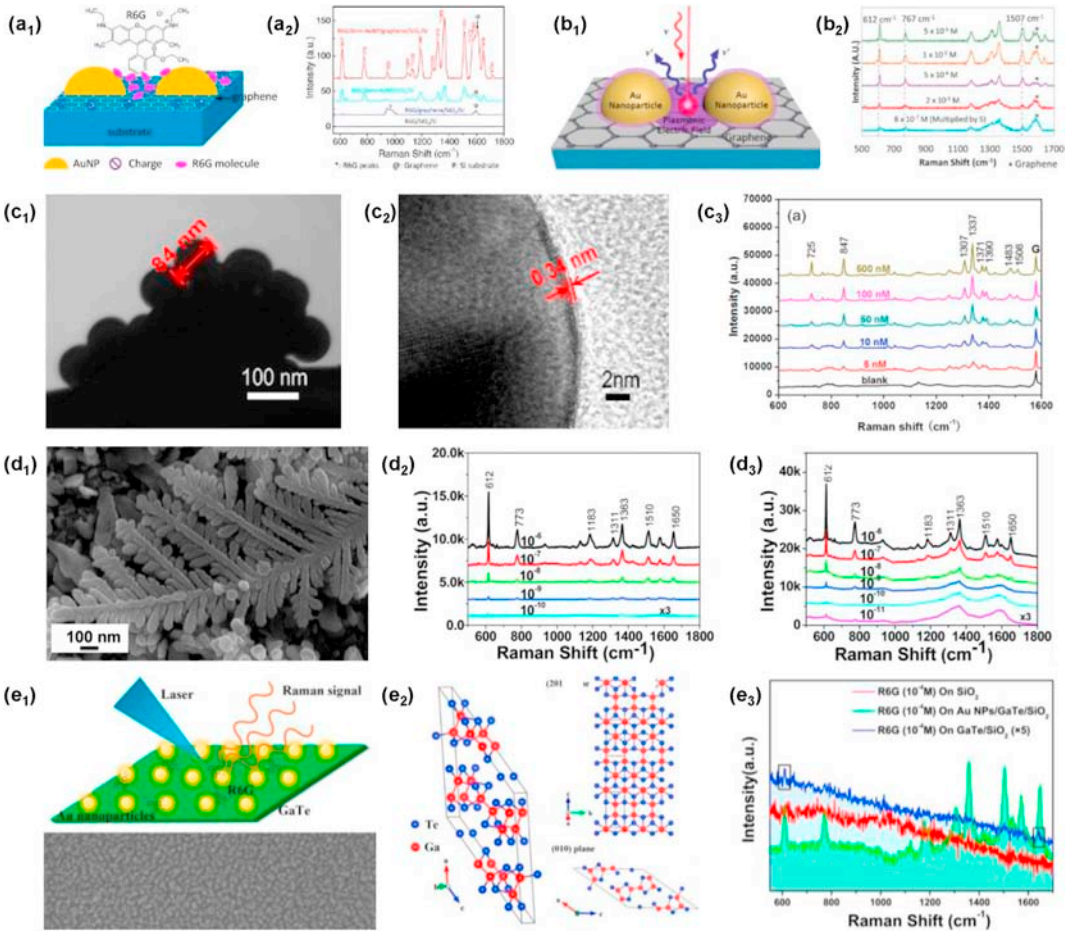

Fig. 7. (a_1) Diagram of R6G molecules deposited on AuNP/graphene SERS substrate. (a_2) Raman spectra for R6G on 8 nm-AuNP/graphene/SiO_2/Si, 8 nm-AuNP/SiO_2/Si, graphene/SiO_2/Si and bare SiO2/Si, respectively. Adapted from Ref. [78], with permission from © 2015 Elsevier Ltd. (b_1) Diagram of plasmonic AuNPs electric field for enhanced Raman scattering. (b_2) Raman spectra of R6G molecules using five different concentrations. Adapted from Ref. [79], with permission from © 2016 Elsevier Ltd. (c_1) TEM image of graphene/CuNPs. (c_2) HRTEM image of cross-sectional monolayer graphene film wrapped on Cu nanoparticles. (c_3) Raman spectra of adenosine in diluted serum with different concentrations. Adapted from Ref. [81], with permission from © 2015 American Chemical Society. (d_1) SEM images of the GO/AgD/Cu substrate. Raman spectra of R6G molecules on the (d_2) AgD/Cu and (d_3) GO/AgD/Cu substrates with different concentrations. Adapted from Ref. [82], with permission from © 2017 The Royal Society of Chemistry. (e_1) Schematic illustration of the R6G molecules on AuNPs/GaTe structure (up) and SEM image (down). (e_2) Left panel: schematic representation of the GaTe crystal structure. Right panel: top view along the direction perpendicular to the (201) plane (up) and the view along the b-axis (down). (e_3) Raman spectra of R6G molecules on different substrates. Adapted from Ref. [37], with permission from © 2017 American Chemical Society.

effect, more complex and artificially structures have been developed through nano-processing. 2D layered materials could be introduced as precise nanospacers between vertical adjacent metallic nanostructures to tremendously generate three-dimensional (3D) hot spots distribution. As shown in Fig. 8a_1 and 8a_2, a 3D Au NPs/graphene/Ag nanohole sandwiched structure with extremely strong electric field enhancement and additional chemical enhancement is considered to be a favorable platform for highly enhanced SERS sensitivity with a detection limit of 10^{-13} M for R6G molecules (Fig. 8a_3) [89]. Furthermore, the directly grown monolayer MoS_2 between adjacent metal NPs acts as the sub-nanometer spacer in AuNP/MoS_2/AuNP (AuMAu) and AgNP/MoS_2/AuNP (AgMAu) hybrid assemblies, providing high-density 3D hot spots [90]. The strong plasmonic couplings contributes significantly to SERS effect with high enhancement factor of 1.98×10^8 and 4.98×10^9 for AuMAu and AgMAu, respectively (Fig. 8b). In addition, Lu et al. reported that the AuNP/WS_2/AuNP substrate with bilayer WS_2 sandwiched between AuNPs shows much better SERS enhancement activity due to high-density 3D hot spots [85]. Tunable nanometer gaps through adjusting the layer number of graphene plays a crucial role in improving the outstanding SERS performance in an AgNPs/graphene@AuNPs system [92]. As the bilayer graphene serves as the vertical nanogaps, the hybrid shows ultrasensitive detection of malachite green (MG) in sea water with the detection limit of 10^{-11} M. Additionally, multilayer hybrid nanostructures using GO film as a nanometer gap between adjacent AgNP layers also exhibit the highly enhanced SERS sensitivity [91]. The hybrid SERS substrate has optimal performance as the number of AgNP layers increases to four (Fig. 8c_1), and the detection limit is down to 10^{-15} M for R6G and 10^{-12} M for crystal violet (Fig. 8c_2 and 8c_3). Although graphene acts as a protection layer that prevents the metallic particles from oxidative damage due to its high impermeability [93,94], it appears to be effective only in the short term [95,96], while it actually accelerates the process of oxidation reaction owing to galvanic corrosion in the long term [97–99]. Compared to graphene, BN is much more inert against oxidation and its wide bandgap makes it an excellent transparent material in the visible and near-IR regions [100,101]. For example, Cai et al. demonstrated that atomically thin BN nanosheets significantly improve the sensitivity, reproducibility, and reusability of SERS substrates with increased Raman signals of two order magnitude [102]. In 2019, Kim et al. demonstrated the effect of the insulating

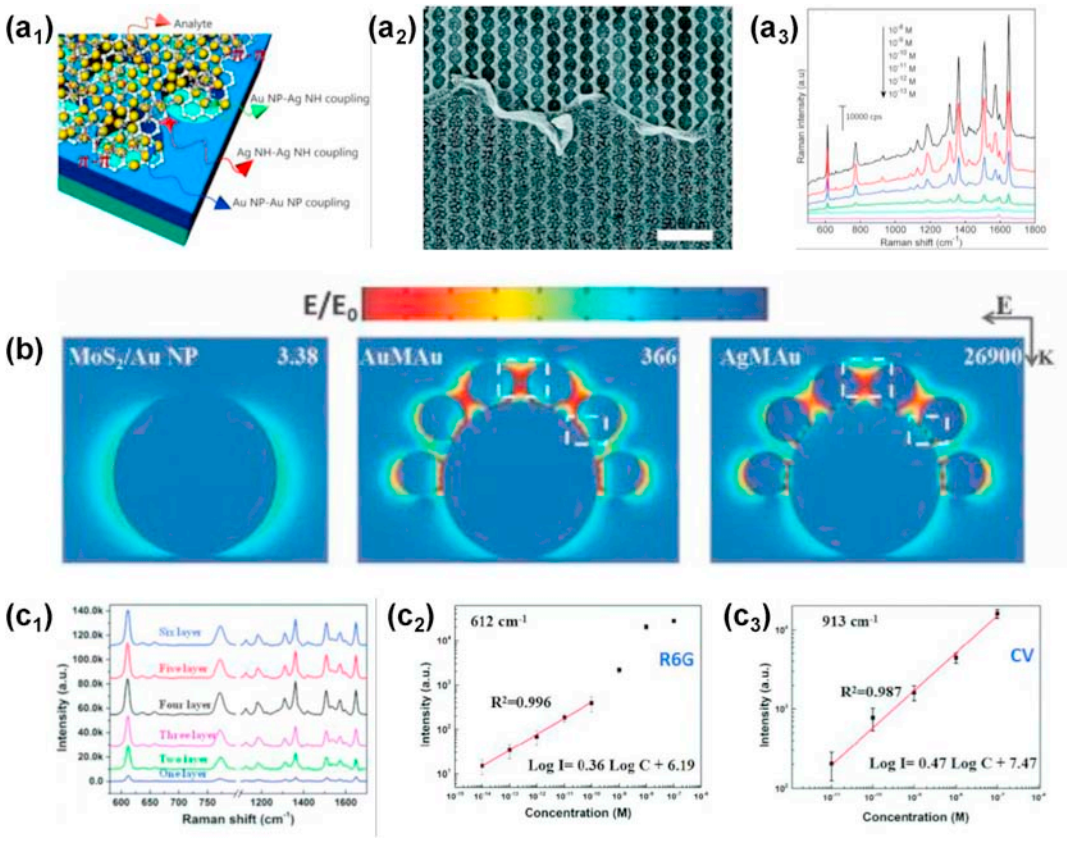

Fig. 8. (a_1) Detection scheme based on the Au NPs/graphene/Ag nanohole sandwiched structure. (a_2) SEM image of the Au NPs/monolayer graphene/Ag nanohole structure. (a_3) SERS spectra of R6G with different molecular concentrations. Adapted from Ref. [89], with permission from © 2017 The Royal Society of Chemistry. (b) Cross-section view of FDTD simulated near-field profile of the electric field intensity distribution for the MoS_2/AuNP, AuMAu, and AgMAu, respectively. Adapted from Ref. [90], with permission from © 2018 WILEY-VCH Verlag GmbH & Co. KGaA, Weinheim. (c_1) The SERS spectra of R6G (10^{-7} M) collected from different AgNP layers. (c_2) The relationship of the SERS intensity at 612 cm^{-1} with R6G molecular concentration. (c_3) The relationship of the SERS intensity at 913 cm^{-1} with the crystal violet molecular concentration. Adapted from Ref. [91], with permission from © 2017 The Royal Society of Chemistry.

property of h-BN on the SERS performance of Au NP/h-BN/Ag NP hybrid platform, which shows superior long-term anti-oxidative stability and enhanced activity than conductive graphene. The detection limit of the h-BN sandwiched substrate is down to 10^{-12} M for R6G solution [103].

The performance of different types of 2D material-based SERS substrates are summarized in Table 1. In general, pristine 2D materials generally possess lower enhancement factors than their engineered counterparts or 2D materials-based heterostructures. However, a more meaningful comparison between different types of SERS platforms would need the same analytes and analysis conditions, including laser wavelength, laser power, accumulation time, etc.

5. Applications of 2D materials-based SERS

Until now, 2D materials have played a prominent role in the development of SERS substrates. Particularly, 2D materials are not only conducive to chemical modification for regulating their biocompatible and electrical properties, but also beneficial to electron transfer for the performance improvement of electronic devices.

Table 1
Summary of different types of 2D material-based SERS substrates.

Type of SERS Substrates	Substrate Materials	Enhancement Factor	Analytes	Ref.
Isotropic	Graphene	2–17	Pc	[43]
2D materials	h-BN	6.9–41	CuPc	[44]
	MoS_2	9.2–108.6	R6G	[62]
Anisotropic	BP	3–6	CuPc	[31]
2D materials	ReS_2	10	CuPc	[59]
2D material van der Waals heterostructures	Graphene/WSe_2	1.6–78.2	CuPc	[32]
	Graphene/ReO_xS_y	150–500	R6G	[68]
2D material/metal heterostructures	AuNPs/graphene	1.19×10^7	R6G	[72]
	GO/AgD	1.6×10^7	R6G	[74]
	Au NPs/MoS_2	1.6×10^4	R6G	[33]
	AuNRs/MXene ($Ti_3C_2T_x$)	4.5×10^6	R6G	[80]
	AuNP/MoS_2/AuNP	1.98×10^8	R6G	[82]
	AuNP/h-BN/AgNP	9.35×10^7	R6G	[95]

Furthermore, 2D materials with high flexibility and transparency attract prospects in wearable smart devices, flexible energy storage devices and other fields. Therefore, high-performance 2D materials-based SERS substrates have a wide range of potential applications in many fields. In this section, we mainly introduce and discuss their applications in the specific niche areas including local strain probing, remote/in-situ chemical analysis, and fine structure characterization.

5.1. Local strain probing

Strain plays a vital role in modulating physical properties of 2D materials-based high-performance devices, especially in flexible and stretchable electronics [104–106]. It strongly modifies not only electronic band structure, but also phonon modes in 2D materials [107]. Particularly, the local strain and surface plasmons can couple at the interface between 2D and plasmonic materials.

A local mechanical strain can be induced by metal deposition on 2D layered materials. Sun et al. demonstrated selective probing of the local strain at the boundaries between metal nanoparticles and MoS_2 layers by the SERS method [108]. Fig. 9a_1 and 9a_3 show the schematic distribution of local strain. For monolayer MoS_2, the local strain can relax in a short distance as the local load can be transferred to the substrate efficiently, while a slower relaxation of strain in the top layer is attributed to a low efficiency of load transfer through the weak interlayer interaction for bilayer MoS_2. After Ag deposition on monolayer MoS_2, both the in-plane E^1_{2g} and out-of-plane A_{1g} vibration modes are split as well as activation of in-plane E_{1g} mode (Fig. 9a_2), which reveals the change of the local electric field after the Ag deposition. However, the effect of mechanical strain becomes much weaker with the increased number of MoS_2 layers (Fig. 9a_4), because the enhanced Raman signals from the less-strained or non-strained lower layers dominate over the signal from the strained top layer. Similarly, Moe et al. utilized the SERS technique to investigate the evolution of local strain at Ag–MoS_2 boundaries (Fig. 9b) [38]. After Ag dendrite deposition on MoS_2, the Raman peaks split (Fig. 9b_1) due to the plasmon-induced localized strain at the Ag–MoS_2 boundaries (Fig. 9b_3). The splitting mode disappears totally over time (Fig. 9b_2) when the plasmon-induced localized strain at the Ag–MoS_2 boundary gradually relaxes into a delocalized strain (Fig. 9b_4). Therefore, the deep understanding of local strain at the metal-2D material boundaries by SERS technique provides a novel route to engineer and characterize 2D materials-based device.

Unlike the strain induced in the Ag–MoS_2 sheet, Hwang et al. reported the evolution of a high local bending strain in MoS_2–Ag nanoscrolls and MoS_2–Au nanoscrolls decorated with metallic nanoparticles using a rolling process (Fig. 9c_1) [109]. Compared to the Raman spectra of the MoS_2 sheets, the Raman peaks become red-shifted and broadened for MoS_2–Ag sheets, MoS_2 and MoS_2–Ag nanoscrolls in the E^1_{2g} and A_{1g} modes (Fig. 9c_2). The E^1_{2g} peak splits into two new peaks with peak shifts of ~4.9 cm^{-1}/% at E^1_{2g-} and ~1.1 cm^{-1}/% strain at E^1_{2g+} for free-standing MoS_2, and the E_{1g} mode appears only in the MoS_2–Ag nanoscrolls (Fig. 9c_3). Moreover, the MoS_2–Ag nanoscrolls result in an induced strain of 2.6% and 1 T-phase of 35% with a SERS enhancement factor of

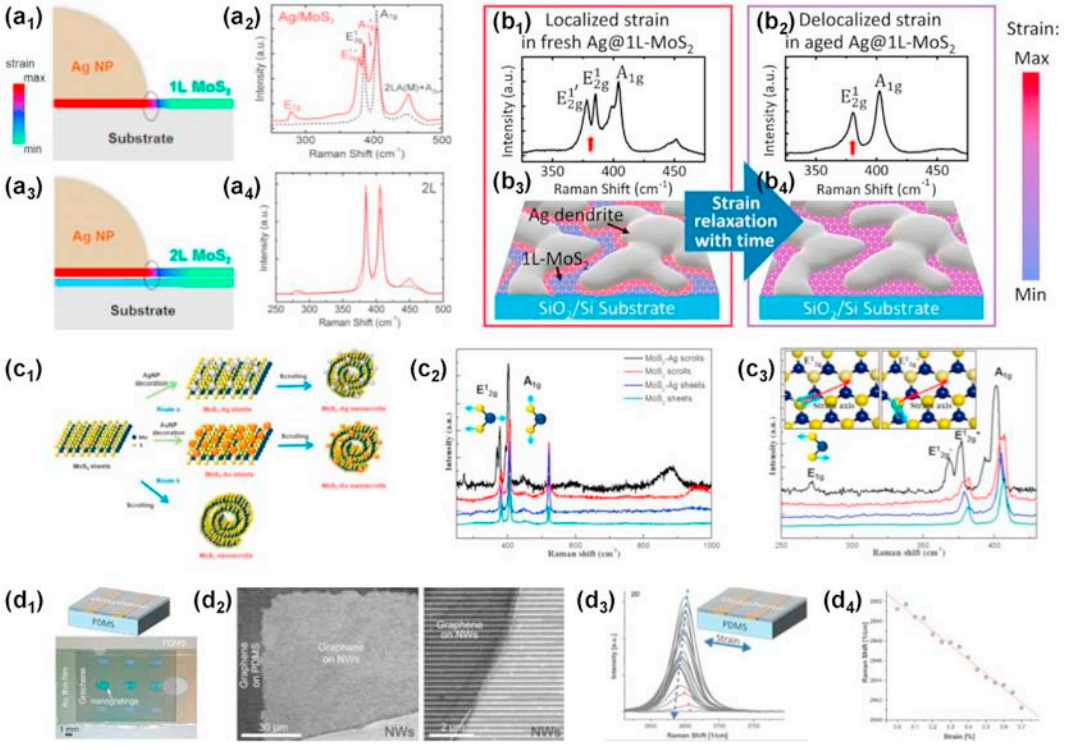

Fig. 9. (a_1–a_4) Schematic diagrams of the distribution of local strain in (a_1) monolayer and (a_3) bilayer MoS_2. Raman spectra of monolayer (a_2) and bilayer (a_4) before (black dash lines) and after Ag deposition (red lines). Adapted from Ref. [108], with permission from © 2014 American Chemical Society. (b_1–b_4) Raman spectra of (b_1) fresh Ag@1 L-MoS_2 and (b_2) aged Ag@1 L-MoS_2 after strain relaxation with time. Illustrations of strain evolution in Ag–1 L MoS_2 heterosystems for (b_3) fresh sample, and (b_4) aged sample with thicker sulfurized Ag layer with a significant strain delocalization. Adapted from Ref. [38], with permission from © 2018 American Chemical Society. (c_1–c_3) (c_1) Schematic processes for scrolling MoS_2 sheets. (c_2) Raman spectra of the MoS_2–Ag nanoscrolls, MoS_2 nanoscrolls, MoS_2–Ag sheets, and MoS_2 sheets, respectively. (c_3) Manifestation of the Raman spectra of MoS_2–Ag nanoscrolls with an tensile strain of about 2.6%. Adapted from Ref. [109], with permission from © 2016 IOP Publishing Ltd. (d_1–d_4) (d_1) Photograph of graphene on nanowire gratings. (d_2) SEM images of transferred graphene on nanowires with partial coverage. (d_3) The Raman 2D band of graphene shifts and broadens in response to the applied strain. (d_4) The corresponding peak position versus strain. Adapted from Ref. [110], with permission from © 2018 WILEY-VCH Verlag GmbH & Co. KGaA, Weinheim.

1.22×10^5.

Additionally, a stretchable metallic nanogratings-graphene coupled structure is used as a SERS substrate for highly sensitive strain sensing [110]. The monolayer graphene is transferred on the flexible substrate with gold nanograting (Fig. 9d_1). The enhanced Raman signal from graphene can be utilized particularly for strain sensing, in which the strain influences the frequency of the Raman phonons that is reflected by peak shift, broadening, and possibly splitting in the Raman spectrum [111]. Fig. 9d_2 shows the partial coverage of graphene on nanogratings. Upon stretching, the Raman 2D band of graphene shifts and broadens with the applied strain (Fig. 9d_3). Fig. 9d_4 shows the linear response to the strain with a sensitivity of -14.24 cm^{-1} $\%^{-1}$ strain.

5.2. Remote/in-situ chemical analysis

Different from the traditional rigid substrate-based SERS detection approach that relies on the extraction of analytes from the targeted surfaces and then their adsorption on desired substrates, flexible SERS sensors are capable of performing the measurement by virtue of the swab-sampling route or even in-situ detection strategy [12,112–114]. Owing to their high optical transparency, flexibility, chemical inertness from external conditions and molecules enricher, 2D materials have been coupled into flexible SERS sensors acting as the multifunctional layers. For instance, 3D hybrid MoS_2/AgNPs/inverted pyramid polymethyl methacrylate (iPPMMA) flexible SERS sensor [40], housed at the end of optical fiber (Fig. 10a_1 and 10a_2), can achieve the detection of complex mixtures solution remotely. The characteristic Raman peaks of each toxic biochemical molecules are easily distinguished (Fig. 10a_3). MoS_2 can act as the protective layer from liquid and atmospheric conditions, showing advantages in real application of biosensing. As opposed to laboratory research applications, the sensitivity of a flexible SERS substrate with an excellent performance is still a grand challenge for practical applications. A 3D flexible plasmonic structure, AgNPs@MoS_2/pyramidal polymer (polymethyl methacrylate), provides a large surface area and can generate dense 3D hot spots (Fig. 10b_1) [115]. The standard melamine solution (a1 in Fig. 10b_2) and mixed solution of melamine and milk (a2 in Fig. 10b_2) with concentrations of 10^{-10}–10^{-4} M and 10^{-6}–10^{-3} M, respectively, are used to validate the SERS performance of the flexible substrate. The 3D AgNPs@MoS_2 activated surface is placed on the surface of the prepared solution (a4 in Fig. 10b_2) for in-situ detection (a3 in Fig. 10b_2). The fingerprint peaks of melamine and MoS_2 are obviously observed with an ultralow detection limit of 10^{-10} M (Fig. 10b_3).

Furthermore, one of the distinct merits of flexible SERS sensors is their capability to be conformally attached onto arbitrary surfaces, rendering the onsite in-situ detection. For instance, Qiu et al. reported PMMA-supported monolayer graphene with sandwiched Ag-nanoflowers (G/AgNFs/PMMA) as flexible SERS substrate using micro-current-assisted chemical reduction method and facile etching process (Fig. 10c_1). Clear Raman signals of trace molecules have been detected by covering the substrate on the real-world surfaces of phenylalanine@apple (Fig. 10c_2), methylene-blue@fish (Fig. 10c_3) and adenosine aqueous solution, respectively. It shows a good suitability for the detection on any arbitrary morphology or aqueous solution surface [116]. In addition, nanogaps are very important for achieving high-density hot spots and optimal SERS enhancement through manipulating LSPRs. However, it represents a significant challenge to form 3D ultra-narrow nanogaps for practical applications. Li and coworkers reported a gyrus-inspired Ag gyrus-nanostructure supported on graphene/Au film for SERS (Fig. 10d_1) [117]. The 3D ultra-narrow nano-gaps (~3 nm) have been achieved between Ag gyrus with the width of ~22 nm (Fig. 10d_2). This flexible SERS substrate has been applied for in-situ detection of MG residue (10^{-11} M) on prawn skin (Fig. 10d_3). Fig. 10d_4 shows the obvious characteristic peaks of MG. Overall, these 2D materials-based flexible SERS platforms present their superior potentials to be intelligently integrated with portable Raman spectroscopy and smart phone technologies for point-of-care diagnostics [112,118].

5.3. Fine structure characterization

2D materials have excellent electronic, optical, physical and chemical features, which depend closely on their fine structures such as the number of layers, edge structures and defects. Therefore, probing these critical structure differences is crucial both for the structural modulation and further applications of 2D materials.

Raman provides a powerful means to probe the structures of 2D materials [65,119]. Usually, the Raman signals of graphene are very weak due to its small portion of scattered radiation, and thus it is hard to effectively differentiate the fine structural characteristics including a low concentration of defects, functional groups, crumpling, and edge structures from the weak Raman spectrum of graphene. Currently, by using the interference-enhanced Raman scattering (IERS) technique, an enhancement ratio of 30 has been obtained for graphene [120], and SERS is another spectroscopic technique with ultrasensitive detection limit, high spatial resolution and high structural selectivity. Consequently, by using a specifically designed substrate of Si/SERS active metal/oxide layer (Fig. 11a)), a surface and interference co-enhanced Raman scattering (SICERS) technique can achieve an enhancement ratio with 10-10^2 times than the sole IERS or SERS technique, and the surface structures and tiny structure change of graphene can be also obtained. The atomic force microscope (AFM) images of graphene on IERS (Fig. 11b) and SICERS substrates (Fig. 11c) indicate that there are some fragments or ribbons on the uneven surface of graphene. Two additional peaks (Fig. 11d) related to the vibrations of fragments or ribbons on the surface of graphene can be determined properly in the Raman spectra of graphene on the SICERS substrate taken with a low laser power. This technique endows SERS with a more powerful tool in the field of ultrasensitive structure characterization in 2D material-based nanoelectronics.

6. Conclusion and outlook

2D materials, a candidate for next-generation information transmission and energy storage devices, play a significant role for SERS by making use of their unique structures and physical/chemical properties. In this review, we have summarized the recent progresses of SERS using diverse 2D layered materials as isolated substrates or as complements to plasmonic SERS substrates. The CM enhancement of 2D materials involved SERS substrates that originates from CT and exciton resonances is introduced. The effect of different symmetries of 2D materials on SERS has been discussed. The in-plane anisotropy of 2D materials not only provides a new way to reveal the fundamental principles of CM process, but also adds up to a new dimension in SERS sensing. Meanwhile, several methods can be utilized to enhance the performances of 2D materials-based SERS substrates, including doping states modification, oxygen incorporation, phase transition engineering and atomic ratio tailoring. Furthermore, 2D materials-based heterostructures as SERS platforms provide superior performance in terms of enhancement factor, limit of detection and stability. Particularly, 2D material/metal heterostructures can induce a much higher enhancement effect than traditional metallic SERS substrates owing to the synergistic effect of EM and CM enhancement. Moreover, the applications of 2D materials-based SERS in niche areas are specifically discussed, including local strain probing,

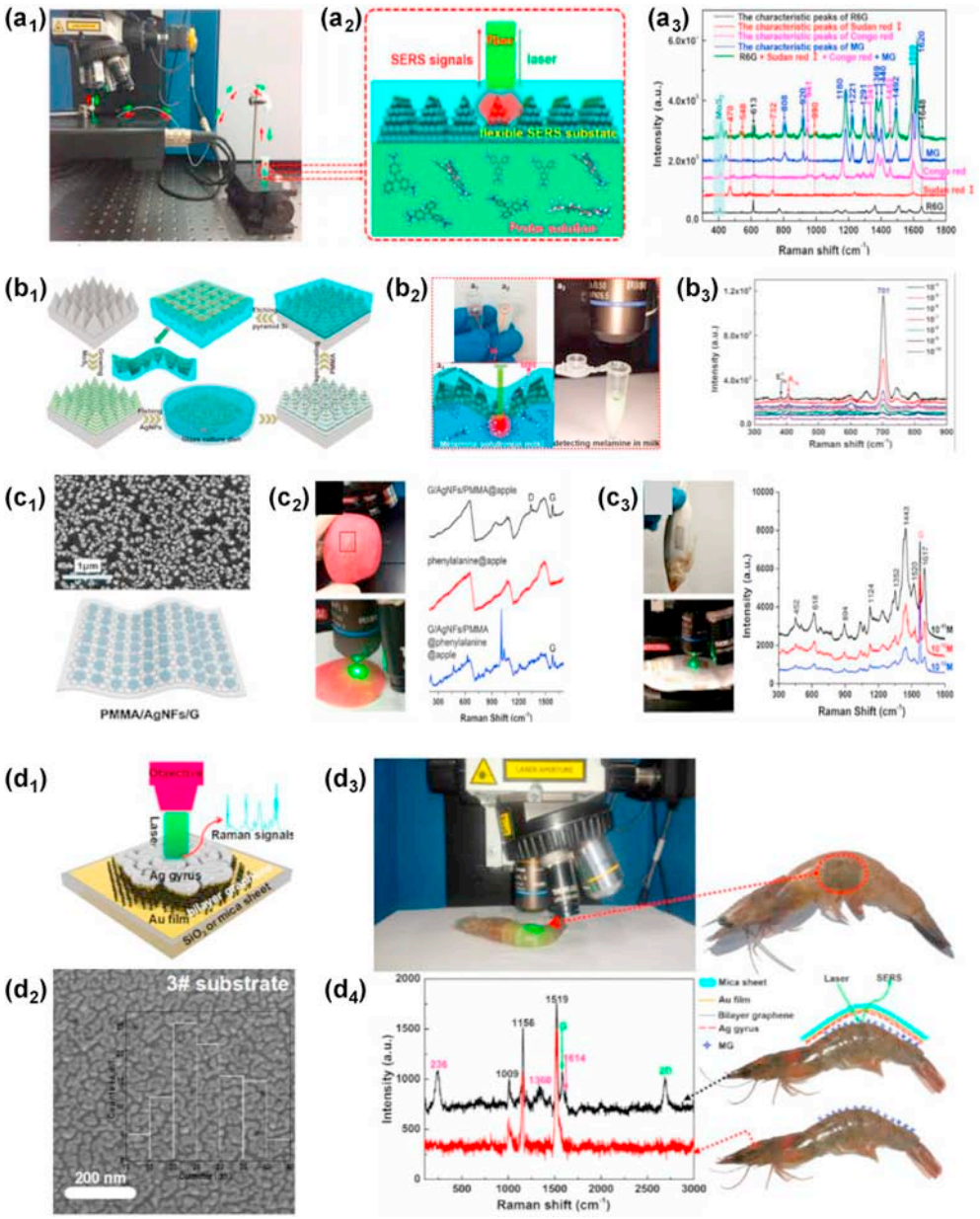

Fig. 10. (a_1) Photograph of remote detecting the mixed molecules. (a_2) The schematic of the partial enlarged detail on the interface between the MoS_2/AgNPs/iPPMMA flexible SERS substrate and the probe solution. (a_3) SERS spectra of R6G (10^{-10} M, black line), Sudan red I (10^{-6} M, red line), congo red (10^{-6} M, pink line), MG (10^{-7} M, blue line) and their mixtures (green line). Adapted from Ref. [40], with permission from © 2018 Elsevier Ltd. (b_1) Schematic of the preparation process of the 3D flexible AgNPs@MoS_2/pyramidal polymer substrate. (b_2) Images of a1) the standard melamine solution, a2) the melamine solution added into milk, a3) the detecting of the melamine solution added into milk, and a4) the schematic of the flexible AgNPs@MoS_2/pyramidal polymer applied for in situ detection of a melamine solution (in milk). (b_3) SERS spectra of the standard melamine solution with a concentration ranging from 10^{-10} to 10^{-4} M. Adapted from Ref. [115], with permission from © 2018 WILEY-VCH Verlag GmbH & Co. KGaA, Weinheim. (c_1) SEM images and schematic of the G/AgNFs/PMMA flexible SERS substrate. (c_2) SERS detection on an apple surface with adsorbed phenylalanine molecules. (c_3) SERS detection on a fish surface with adsorbed methylene-blue molecules. Adapted from Ref. [116], with permission from © 2017 Elsevier Ltd. (d_1) Schematic and (d_2) SEM image of the Ag-gyrus/graphene/Au film substrate. (d_3) The picture of the in situ detection of MG (10^{-11} M) on prawn skin, and (d_4) corresponding SERS spectrawith (black curve) and without (red curve) the flexible substrate. Adapted from Ref. [117], with permission from © 2017 Optical Society of America.

remote/in-situ chemical analysis, and fine structure characterization.

Although there has been great progress in using 2D materials as a multi-functional agent for high-performance SERS substrates and being implemented in a more elaborate design way, the practical applications of this technique are still at an early stage and many challenges remain. Here, we envision several directions to further advance the development of this booming field: (i) More studies are needed to obtaining a deep insight into the fundamental mechanisms of 2D materials-based SERS, such as the polaritons' behavior, the crystal orientation and thickness dependence of 2D materials; (ii) The modeling tools and standardization protocols are generally required for the characterization of 2D materials-based SERS substrates and more reliable, quantitative determination of SERS performance, such as electrodynamic model or multiplicative effects model; (iii) New approaches must be developed to facilitate the nondestructive integration of multiple 2D materials into a SERS platform in order to improve the sensitivity, stability, and reproducibility; (iv) To engineer the intrinsic physicochemical properties of 2D materials for practical applications, the surface modification

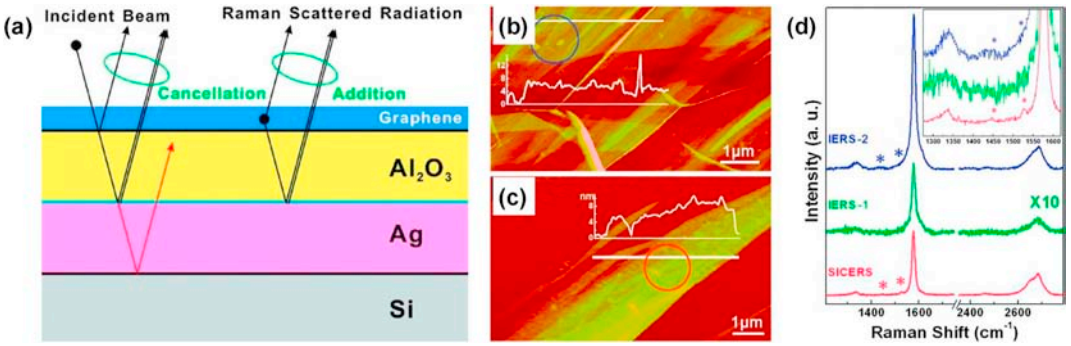

Fig. 11. (a) Schematic of laser penetrating through a typical Si capped with surface-active metal and oxide double layers substrate of Si/Ag/Al_2O_3 with graphene on it. AFM images of graphene (b) on an IERS substrate (Si/285 nm SiO_2) and (c) on a SICERS substrate. (d) Raman spectra of graphene on the IERS and SICERS substrates. The inset shows the details of two additional peaks about 1450 and 1530 cm^{-1}. Adapted from Ref. [39], with permission from © 2009 American Chemical Society.

or functionalization of 2D materials, such as surface incorporation or defect engineering, is a necessity; (v) The interdisciplinary strategies from fields of synthetic chemistry and materials engineering are suggested to expand SERS in new directions.

Declaration of competing interest

All authors declare no conflict of interest of this manuscript.

Acknowledgments

This work was supported in part by National Natural Science Foundation of China (Grant No. 62075093, 61805113), Natural Science Foundation of Guangdong Province (Grant No. 2018A030310224), Guangdong Innovative and Entrepreneurial Research Team Program (Grant No. 2017ZT07C071), and Shenzhen Science and Technology Innovation Commission (Grant No. GJHZ20180928155207206, JCYJ20170817111349280, and JCYJ20180305180635082).

References

[1] B. Zou, Y. Chen, Y. Liu, R. Xie, Q. Du, T. Zhang, Y. Shen, B. Zheng, S. Li, J. Wu, Weina Zhang, W. Huang, X. Huang, F. Huo, Adv. Sci. 6 (2019) 1801283.
[2] K. Xu, Y. Lu, K. Takei, Adv. Mater. Technol. 4 (2019) 1800628.
[3] K. Xu, Y. Lu, S. Honda, T. Arie, S. Akita, K. Takei, J. Mater. Chem. C 7 (2019) 9609.
[4] Y. Lee, J. Kim, H. Joo, M.S. Raj, R. Ghaffari, D.-H. Kim, Adv. Mater. Technol. 2 (2017) 1700053.
[5] S.M. Nie, S.R. Emery, Science 275 (1997) 1102.
[6] A. Campion, P. Kambhampati, Chem. Soc. Rev. 27 (1998) 241.
[7] M. Moskovits, B.D. Piorek, J. Raman Spectrosc. 52 (2021) 279.
[8] L. Guerrini, D. Graham, Chem. Soc. Rev. 41 (2012) 7085.
[9] J. Liu, H. He, D. Xiao, S. Yin, W. Ji, S. Jiang, D. Luo, B. Wang, Y. Liu, Materials 11 (2018) 1833.
[10] J.M. Nam, J.W. Oh, H. Lee, Y.D. Suh, Acc. Chem. Res. 49 (2016) 2746.
[11] K. Xu, H. Yan, C.F. Tan, Y. Lu, Y. Li, G.W. Ho, R. Ji, M. Hong, Adv.Opt. Mater. 6 (2018) 1701167.
[12] K. Xu, Z. Wang, C.F. Tan, N. Kang, L. Chen, L. Ren, E.S. Thian, G.W. Ho, R. Ji, M. Hong, ACS Appl. Mater. Interfaces 9 (2017) 26341.
[13] J. Song, W. Nam, W. Zhou, Adv. Mater. Technol. 4 (2019) 1800689.
[14] L. Yang, Y. Peng, Y. Yang, J. Liu, H. Huang, B. Yu, J. Zhao, Y. Lu, Z. Huang, Z. Li, J.R. Lombardi, Adv. Sci. 6 (2019) 1900310.
[15] K.N. Kanipe, P.P.F. Chidester, G.D. Stucky, M. Moskovits, ACS Nano 10 (2016) 7566.
[16] A.M. Michaels, M. Nirmal, L.E. Brus, J. Am. Chem. Soc. 121 (1999) 9932.
[17] W.J. Cho, Y. Kim, J.K. Kim, ACS Nano 6 (1) (2012) 249.
[18] K. Xu, C. Zhang, T.H. Lu, P. Wang, R. Zhou, R. Ji, M. Hong, Opto-Electronic Eng. 44 (2017) 185.
[19] B. Liu, D. Zhang, H. Ni, D. Wang, L. Jiang, D. Fu, X. Han, C. Zhang, H. Chen, Z. Gu, ACS Appl. Mater. interfaces 10 (2017) 21.
[20] X. Wang, X. Zhu, H. Shi, Y. Chen, Z. Chen, Y. Zeng, Z. Tang, H. Duan, ACS Appl. Mater. Interfaces 10 (41) (2018) 35607.
[21] K. Xu, C. Zhang, R. Zhou, R. Ji, M. Hong, Optic Express 24 (2016) 10352.
[22] Z. Zheng, S. Cong, W. Gong, J. Xuan, G. Li, W. Lu, F. Geng, Z. Zhao, Nat. Commun. 8 (2017) 1993.
[23] W. Xu, X. Ling, J. Xiao, M.S. Dresselhaus, J. Kong, H. Xu, Z. Liu, J. Zhang, Proc. Natl. Acad. Sci. U. S. A. 109 (2012) 9281.
[24] S.J. Hurst, H.C. Fry, D.J. Gosztola, T. Rajh, J. Phys. Chem. C 115 (2011) 620.
[25] A. Musumeci, D. Gosztola, T. Schiller, N.M. Dimitrijevic, V. Mujica, D. Martin, T. Rajh, J. Am. Chem. Soc. 131 (2009) 6040.
[26] C. Lian, S.Q. Hu, J. Zhang, C. Cheng, Z. Yuan, S. Gao, S. Meng, Phys. Rev. Lett. 125 (2020) 116802.
[27] S.A. Ghopry, M.A. Alamri, R. Goul, R. Sakidja, J.Z. Wu, Adv. Opt. Mater. 7 (2019) 1801249.
[28] S.A. Ghopry, M. Alamri, R. Goul, B. Cook, S. Sadeghi, R. Gutha, R. Sakidja, J.Z. Wu, ACS Appl. Nano Mater. 3 (2020) 2354.
[29] K.S. Novoselov, A.K. Geim, S.V. Morozov, D. Jiang, Y. Zhang, S.V. Dubonos, I.V. Grigorieva, A.A. Firsov, Science 306 (2004) 666.
[30] I. Alessandri, J.R. Lombardi, Chem. Rev. 116 (2016) 14921.
[31] P. Karthick Kannan, P. Shankar, C. Blackman, C.H. Chung, Adv. Mater. (2019): e1803432.
[32] W. Xu, N. Mao, J. Zhang, Small 9 (2013) 1206.
[33] N. Zhang, L. Tong, J. Zhang, Chem. Mater. 28 (2016) 6426.
[34] X. Ling, S. Huang, S. Deng, N. Mao, J. Kong, M. S Dresselhaus, J. Zhang, Acc. Chem. Res. 48 (2015) 1862.
[35] J.J. Lin, L.B. Liang, X. Ling, S.Q. Zhang, N.N. Mao, N. Zhang, B.G. Sumpter, V. Meunier, L.M. Tong, J. Zhang, J. Am. Chem. Soc. 137 (2015) 15511.
[36] Y. Tan, L.N. Ma, Z.B. Gao, M. Chen, F. Chen, Nano Lett. 17 (2017) 2621.
[37] P.Q. Lu, J.W. Lang, Z.P. Weng, A. Rahimi-Iman, H.Z. Wu, ACS Appl. Mater. Interfaces 10 (2018) 1356.
[38] Y.A. Moe, Y. Sun, H. Ye, K. Liu, R. Wang, ACS Appl. Mater. Interfaces 10 (2018) 40246.
[39] L.B. Gao, W.C. Ren, B.L. Liu, R. Saito, Z.S. Wu, S.S. Li, C.B. Jiang, F. Li, H.M. Cheng, ACS Nano 3 (2009) 933.
[40] C.H. Li, S.C. Xu, J. Yu, S.Z. Jiang, A.H. Liu, Z. Li, S.Z. Zhang, X.F. Zhao, C. Zhang, B.Y. Man, Sensor. Actuator. B Chem. 274 (2018) 152.
[41] J.R. Lombardi, R.L. Birke, Accounts Chem. Res. 42 (6) (2009) 734.
[42] G. Demirel, H. Usta, M. Yilmaz, M. Celik, H.A. Alidagi, F. Buyukserin, J. Mater. Chem. C 6 (2018) 5314.
[43] X.X. Han, W. Ji, B. Zhao, Y. Ozaki, Nanoscale 9 (2017) 4847.
[44] P. Miao, J.K. Qin, Y. Shen, H. Su, J. Dai, B. Song, Y. Du, M. Sun, W. Zhang, H.L. Wang, C.Y. Xu, P. Xu, Small 14 (2018) 1704079.
[45] J.R. Lombardi, R.L. Birke, J. Phys. Chem. C 118 (2014) 11120.
[46] K.S. Novoselov, D. Jiang, F. Schedin, T.J. Booth, V.V. Khotkevich, S.V. Morozov, A.K. Geim, Proc. Natl. Acad. Sci. U.S.A. 102 (2005) 10451.
[47] X.L. Li, W.P. Han, J.B. Wu, X.F. Qiao, J. Zhang, P.H. Tan, Adv. Funct. Mater. 27 (2017) 1604468.
[48] X. Ling, L.M. Xie, Y. Fang, H. Xu, H.L. Zhang, J. Kong, M.S. Dresselhaus, J. Zhang, Z.F. Liu, Nano Lett. 10 (2010) 553.
[49] X. Ling, J. Zhang, Small 6 (2010) 2020.
[50] H. Xu, L.M. Xie, H.L. Zhang, J. Zhang, ACS Nano 5 (2011) 5338.
[51] H. Xu, Y. Chen, W. Xu, H. Zhang, J. Kong, M.S. Dresselhaus, J. Zhang, Small 7 (2011) 2945.
[52] H.T. Liu, Y.Q. Liu, D.B. Zhu, J. Mater. Chem. 21 (2011) 3335.
[53] J.E. Rowe, C.V. Shank, D.A. Zwemer, C.A. Murray, Phys. Rev. Lett. 44 (1980) 1770.
[54] I. Gierz, C. Riedl, U. Starke, C.R. Ast, K. Kern, Nano Lett. 8 (2008) 4603.
[55] X. Ling, W. Fang, Y.H. Lee, P.T. Araujo, X. Zhang, J.F. Rodriguez-Nieva, Y. Lin, J. Zhang, J. Kong, M.S. Dresselhaus, Nano Lett. 14 (2014) 3033.
[56] A. Splendiani, L. Sun, Y.B. Zhang, T.S. Li, J. Kim, C.Y. Chim, G. Galli, F. Wang, Nano Lett. 10 (2010) 1271.
[57] P. Zuo, L. Jiang, X. Li, P. Ran, B. Li, A. Song, M. Tian, T. Ma, B. Guo, L. Qu, Y. Lu, Nanoscale 11 (2019) 485.
[58] R. Anbazhagan, A. Vadivelmurugan, H.-C. Tsai, R.-J. Jeng, J. Mater. Chem.C 6 (2018) 1071.
[59] M. Chen, B. Ji, Z. Dai, X. Du, B. He, G. Chen, D. Liu, S. Chen, K.H. Lo, S. Wang,

B. Zhou, H. Pan, Appl. Surf. Sci. 527 (2020) 146769.
[60] X. Li, J. Li, X. Zhou, Y. Ma, Z. Zheng, X. Duan, Y. Qu, Carbon 66 (2014) 713.
[61] M. Chen, D. Liu, X. Du, K.H. Lo, S. Wang, B. Zhou, H. Pan, Trends Anal. Chem. 130 (2020) 115983.
[62] L.K. Li, Y.J. Yu, G.J. Ye, Q.Q. Ge, X.D. Ou, H. Wu, D.L. Feng, X.H. Chen, Y.B. Zhang, Nat. Nanotechnol. 9 (2014) 372.
[63] S. Tongay, H. Sahin, C. Ko, A. Luce, W. Fan, K. Liu, J. Zhou, Y.S. Huang, C.H. Ho, J.Y. Yan, D.F. Ogletree, S. Aloni, J. Ji, S.S. Li, J.B. Li, F.M. Peeters, J.Q. Wu, Nat. Commun. 5 (2014) 3252.
[64] D.A. Chenet, O.B. Aslan, P.Y. Huang, C. Fan, A.M. van der Zande, T.F. Heinz, J.C. Hone, Nano Lett. 15 (2015) 5667.
[65] J.X. Wu, N.N. Mao, L.M. Xie, H. Xu, J. Zhang, Angew. Chem. Int. Ed. 54 (2015) 2366.
[66] X.M. Wang, A.M. Jones, K.L. Seyler, V. Tran, Y.C. Jia, H. Zhao, H. Wang, L. Yang, X.D. Xu, F.N. Xia, Nat. Nanotechnol. 10 (2015) 517.
[67] C.H. Ho, Y.S. Huang, K.K. Tiong, P.C. Liao, J. Phys. Condens. Matter 11 (1999) 5367.
[68] S.M. Feng, M.C. dos Santos, B.R. Carvalho, R.T. Lv, Q. Li, K. Fujisawa, A.L. Elias, Y. Lei, N. Perea-Lopez, M. Endo, M.H. Pan, M.A. Pimenta, M. Terrones, Sci. Adv. 2 (2016): e1600322.
[69] Y. Yin, P. Miao, Y.M. Zhang, J.C. Han, X.H. Zhang, Y. Gong, L. Gu, C.Y. Xu, T. Yao, P. Xu, Y. Wang, B. Song, S. Jin, Adv. Funct. Mater. 27 (2017) 1606694.
[70] X. Song, Y. Wang, F. Zhao, Q. Li, H.Q. Ta, M.H. Rummeli, C.G. Tully, Z. Li, W.J. Yin, L. Yang, K.B. Lee, J. Yang, I. Bozkurt, S. Liu, W. Zhang, M. Chhowalla, ACS Nano 13 (2019) 8312.
[71] Y.R. Liu, Z.B. Gao, M. Chen, Y. Tan, F. Chen, Adv. Funct. Mater. 28 (2018) 1805710.
[72] X. Hou, X. Zhang, Q. Ma, X. Tang, Q. Hao, Y. Cheng, T. Qiu, Adv. Funct. Mater. 30 (2020) 1910171.
[73] Y. Liu, Z. Gao, Y. Tan, F. Chen, ACS Nano 12 (2018) 10529.
[74] Z.Y. Cai, B.L. Liu, X.L. Zou, H.M. Cheng, Chem. Rev. 118 (2018) 6091.
[75] T. Georgiou, R. Jalil, B.D. Belle, L. Britnell, R.V. Gorbachev, S.V. Morozov, Y.J. Kim, A. Gholinia, S.J. Haigh, O. Makarovsky, L. Eaves, L.A. Ponomarenko, A.K. Geim, K.S. Novoselov, A. Mishchenko, Nat. Nanotechnol. 8 (2013) 100.
[76] J. Seo, J. Lee, Y. Kim, D. Koo, G. Lee, H. Park, Nano Lett. 20 (2020) 1620.
[77] M. Dandu, K. Watanabe, T. Taniguchi, A.K. Sood, K. Majumdar, ACS Photonics 7 (2020) 519.
[78] R.T. Lu, A. Konzelmann, F. Xu, Y.P. Gong, J.W. Liu, Q.F. Liu, M. Xin, R.Q. Hui, J.Z. Wu, Carbon 86 (2015) 78.
[79] R. Goul, S. Das, Q.F. Liu, M. Xin, R.T. Lu, R. Hui, J.Z. Wu, Carbon 111 (2017) 386.
[80] W.J. Chen, X.C. Gui, Y.J. Zheng, B.H. Liang, Z.Q. Lin, C.C. Zhao, H.J. Chen, Z.F. Chen, X.M. Li, Z.K. Tang, Adv. Opt. Mater. 5 (2017) 1600715.
[81] S.C. Xu, B.Y. Man, S.Z. Jiang, J.H. Wang, J. Wei, S.D. Xu, H.P. Liu, S.B. Gao, H.L. Liu, Z.H. Li, H.S. Li, H.W. Qin, ACS Appl. Mater. Interfaces 7 (2015) 10977.
[82] L.T. Hu, Y.J. Liu, Y.S. Han, P.X. Chen, C. Zhang, C.H. Li, Z.Y. Lu, D. Luo, S.Z. Jiang, J. Mater. Chem. C 5 (2017) 3908.
[83] J.F. Li, Y.F. Huang, Y. Ding, Z.L. Yang, S.B. Li, X.S. Zhou, F.R. Fan, W. Zhang, Z.Y. Zhou, D.Y. Wu, B. Ren, Z.L. Wang, Z.Q. Tian, Nature 464 (2010) 392.
[84] C. Zhang, S.Z. Jiang, Y.Y. Huo, A.H. Liu, S.C. Xu, X.Y. Liu, Z.C. Sun, Y.Y. Xu, Z. Li, B.Y. Man, Optic Express 23 (2015) 24811.
[85] Z.Y. Lu, H.P. Si, Z. Li, J. Yu, Y.J. Liu, D.J. Feng, C. Zhang, W. Yang, B.Y. Man, S.Z. Jiang, Optic Express 26 (2018) 21626.
[86] J.P. Lu, J.H. Lu, H.W. Liu, B. Liu, L.L. Gong, E.S. Tok, K.P. Loh, C.H. Sow, Small 11 (2015) 1792.
[87] Z. Li, S.Z. Jiang, Y.Y. Huo, M. Liu, C. Yang, C. Zhang, X.Y. Liu, Y.Q. Sheng, C.H. Li, B.Y. Man, Optic Express 24 (2016) 26097.
[88] H. Xie, P. Li, J. Shao, H. Huang, Y. Chen, Z. Jiang, P.K. Chu, X.F. Yu, ACS Sens. 4 (2019) 2303.
[89] Y. Zhao, D. Yang, X.Y. Li, Y. Liu, X. Hu, D.F. Zhou, Y.L. Lu, Nanoscale 9 (2017) 1087.
[90] Z. Li, S.Z. Jiang, Y.Y. Huo, A.H. Liu, C. Zhang, J. Yu, M.H. Wang, C.H. Li, Z.Y. Lu, B.Y. Man, Adv. Mater. Interfaces 5 (2018) 1800661.
[91] C.H. Zhang, J. Lia, S. Yu, Z. Jiang, S.C. Xu, C. Yang, Y.J. Liu, X.G. Gao, A.H. Liu, B.Y. Man, Sensor. Actuator. B Chem. 258 (2018) 163.
[92] S.Z. Li, Y.Y. Jiang, Huo, T.Y. Ning, A.H. Liu, C. Zhang, Y. He, M.H. Wang, C.H. Li, B.Y. Man, Nanoscale 10 (2018) 5897.
[93] Y. Li, J. Li, X.M. Zhou, Y.Y. Ma, Z.P. Zheng, X.F. Duan, Y.Q. Qu, Carbon 66 (2014) 713.
[94] I. Bergmair Losurdo, B. Dastmalchi, T.H. Kim, M.M. Giangregroio, W.Y. Jiao, G.V. Bianco, A.S. Brown, K. Hingerl, G. Bruno, Adv. Funct. Mater. 24 (2014) 1864.
[95] J. C. Tuberquia Prasai, R.R. Harl, G.K. Jennings, K.I. Bolotin, ACS Nano 6 (2012) 1102.
[96] S. Chen, L. Brown, M. Levendorf, W.W. Cai, S.Y. Ju, J. Edgeworth, X.S. Li, C.W. Magnuson, A. Velamakanni, R.D. Piner, J.Y. Kang, J. Park, R.S. Ruoff, ACS Nano 5 (2011) 1321.
[97] Z.T. Zhou, G. Li, J. Shenoy, L. Li, H.T. Liu, ACS Nano 7 (2013) 6939.
[98] W. Regan Schriver, W.J. Gannett, A.M. Zaniewski, M.F. Crommie, A. Zettl, ACS Nano 7 (2013) 5763.
[99] L.H. Li, T. Xing, Y. Chen, R. Jones, Adv. Mater. Interfaces 1 (2014) 1300132.
[100] Y. Lin, T.V. Williams, J.W. Connell, J. Phys. Chem. Lett. 1 (2010) 277.
[101] D. Chugh, C. Jagadish, H. Tan, Adv. Mater. Technol. 4 (2019) 1900220.
[102] Q.R. Cai, S. Mateti, W.R. Yang, R. Jones, K. Watanabe, T. Taniguchi, S.M. Huang, Y. Chen, L.H. Li, Angew. Chem. Int. Ed. 55 (2016) 8405.
[103] N.Y. Kim, Y.C. Leem, S.H. Hong, J.H. Park, S.Y. Yim, ACS Appl. Mater. Interfaces 11 (2019) 6363.
[104] J. Pu, Y. Yomogida, K.K. Liu, L.J. Li, Y. Iwasa, T. Takenobu, Nano Lett. 12 (2012) 4013.
[105] H.Y. Chang, S.X. Yang, J.H. Lee, L. Tao, W.S. Hwang, D. Jena, N.S. Lu, D. Akinwande, ACS Nano 7 (2013) 5446.
[106] J. Yoon, W. Park, G.Y. Bae, Y. Kim, H.S. Jang, Y. Hyun, S.K. Lim, Y.H. Kahng, W.K. Hong, B.H. Lee, H.C. Ko, Small 9 (2013) 3295.
[107] H.J. Conley, B. Wang, J.I. Ziegler, R.F. Haglund, S.T. Pantelides, K.I. Bolotin, Nano Lett. 13 (2013) 3626.
[108] Y.H. Sun, K. Liu, X.P. Hong, M. Chen, J. Kim, S.F. Shi, J.Q. Wu, A. Zettl, F. Wang, Nano Lett. 14 (2014) 5329.
[109] D.Y. Hwang, D.H. Suh, Nanotechnology 28 (2017): 025603.
[110] R.F. Tiefenauer, T. Dalgaty, T. Keplinger, T. Tian, C.J. Shih, J. Voros, M. Aramesh, Small 14 (2018) 1801187.
[111] O. Frank, G. Tsoukleri, I. Riaz, K. Papagelis, J. Parthenios, A.C. Ferrari, A.K. Geim, K.S. Novoselov, C. Galiotis, Nat. Commun. 2 (2011) 256.
[112] K. Xu, R. Zhou, K. Takei, M. Hong, Adv. Sci. 6 (2019) 1900925.
[113] X. Lin, X.-T. Lou, D.-Y. Lin, Z.-W. Lu, Phys. Chem. Chem. Phys. 17 (2015) 31324.
[114] W. Wei, Y. Du, L. Zhang, Y. Yang, Y. Gao, J. Mater. Chem. C 6 (2018) 8793.
[115] C. Li, J. Yu, S. Xu, S. Jiang, X. Xiu, C. Chen, A. Liu, T. Wu, B. Man, C. Zhang, Adv. Mater. Technol. 3 (2018) 1800174.
[116] H.W. Qiu, M.Q. Wang, S.Z. Jiang, L. Zhang, Z. Yang, L. Li, J.J. Li, M.H. Cao, J. Huang, Sensor. Actuator. B Chem. 249 (2017) 439.
[117] C. Li, A. Liu, C. Zhang, M. Wang, Z. Li, S. Xu, S. Jiang, J. Yu, C. Yang, B. Man, Optic Express 25 (2017) 20631.
[118] T. Mu, S. Wang, T. Li, B. Wang, X. Ma, B. Huang, L. Zhu, J. Guo, IEEE J. Sel. Top. Quant. Electron. 25 (2018) 1.
[119] A.C. Ferrari, J.C. Meyer, V. Scardaci, C. Casiraghi, M. Lazzeri, F. Mauri, S. Piscanec, D. Jiang, K.S. Novoselov, S. Roth, A.K. Geim, Phys. Rev. Lett. 97 (2006) 187401.
[120] Y.Y. Wang, Z.H. Ni, Z.X. Shen, H.M. Wang, Y.H. Wu, Appl. Phys. Lett. 92 (2008): 43121.